Hindawi
Journal of Nanomaterials
Volume 2022, Article ID 6825524, 8 pages
https://doi.org/10.1155/2022/6825524

Research Article

UPLC-ESI-TOF-MS Analysis of the Effect of Dendrimers Core Lengths on Their Molecular Profiles and Purity

Hosam Gharib Abdelhady,[1,2] **Fadilah Sfouq Aleanizy**,[3] **Fulwah Yahya Alqahtani**,[3] **and Hamad Alkahtani**[4]

[1]*Department of Physiology and Pharmacology, Sam Houston State University College of Osteopathic Medicine, 925 City Central Avenue, Conroe, TX 77304, USA*
[2]*Department of Pharmaceutics and Pharmaceutical Technology, College of Pharmacy, Taibah University, Al-Madinah Al-Munawwarah 42331, Saudi Arabia*
[3]*Department of Pharmaceutics, College of Pharmacy, King Saud University, Riyadh, Saudi Arabia*
[4]*Department of Pharmaceutical Chemistry, College of Pharmacy, King Saud University, Riyadh, Saudi Arabia*

Correspondence should be addressed to Hosam Gharib Abdelhady; habdelhady@lecom.edu

Received 29 September 2021; Accepted 30 March 2022; Published 24 May 2022

Academic Editor: Antonios Kelarakis

The effect of core length of Polyamidoamine (PAMAM) dendrimers on their physicochemical properties and hence their purity was studied by ultraperformance liquid chromatography-electrospray ionization-time of flight-mass spectrometry (UPLC-ESI-TOF-MS). Seven consecutive generations $G_n = (G_{0\text{-}6})$ of both Ethylenediamine core (C_2) and Diaminobutane core (C_4) dendrimers were tested. The separation and detection of each generation of dendrimers (covering a molar mass range of 517-58,076 Da and a radius range of 15-67 Å) were performed within 10 min. Increasing the length of the core by the C_2H_4 group significantly changed the morphological characteristics of the dendrimers. For example, the general morphology of C_4 dendrimers becomes less compact than C_2 dendrimers. This facilitates the influx of impurities from the inner nanocavities of these molecules, even at higher generations, during the UPLC run providing C_4 dendrimers of higher purity than C_2 dendrimers. These results reveal that the toxicity found by some researchers due to the application of dendrimers may be mostly due to leakage of the encapsulated starting materials, which can be eliminated by using optimized dendritic molecules.12

1. Introduction

Polyamidoamine (PAMAM) dendrimers [1] have been successfully used as delivery nanomolecules for treating neurological diseases [2], gene therapy [3–7], magnetic resonance imaging contrast agents [8], and as scaffolds for biomimetic systems [9]. These dendrimers were considered soft super atoms with controlled size, shape, and tunable surface chemistry [10–13]. While PAMAM dendrimers are relatively monodispersed, however, they may show some defects leading to polydispersity. These defects may vary with the dendrimer core length and generation size. Therefore, efficient analytical methods are required to characterize and examine the molecular weight distribution and purity of these dendrimers. To this end, ultraperformance liquid chromatography (UPLC) have been used to separate and characterize the purity of different types of PAMAM dendrimers [14–16]. Application of UPLC has increased the average number of theoretical plates, improved resolution efficiencies, and reduced sample elution times [17]. The dendrimers characterized here contain either ethylenediamine (C_2) or a diaminobutane (C_4) initiator cores. Both dendrimers contain repeat monomer units of PAMAM

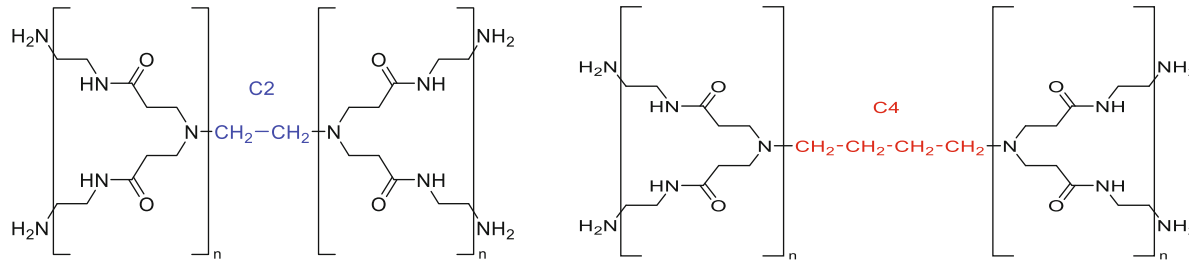

(a) (b)

Scheme 1: C_2 (a) and C_4 (b) PAMAM dendrimers, n = generation number.

(-$CH_2CH_2CONHCH_2CH_2N$-) and primary amine terminal groups (NH_2) as shown in Scheme 1.

We demonstrate the applicability of UPLC with the electrospray ionization-time-of-flight-mass spectrometer (UPLC-ESI-TOF-MS) to study the effect of increasing the length of the dendritic core, by a small C_2H_4 molecule, on the physical properties and the purity of zero to six generation (G_0-G_6) C_2 and C_4 PAMAM dendrimers. The intrinsic basic nature of these molecules makes them ideal samples for ESI-MS due to the production of many multiple charged ions [18, 19]. The application of UPLC-ESI-TOF-MS provides rapid separation, ionization, and characterization techniques. To our knowledge, this is the first study that includes UPLC-ESI-TOF-MS characterization to determine dendrimers purity based on their core lengths.

2. Materials and Methods

2.1. Materials. All chemicals were obtained from Aldrich (Milwaukee, WI, USA). Seven generations (G_n =0-6) of each of C_2 and C_4 PAMAM Dendrimers were used. DI water was obtained using the Milli-Q plus system (Millipore, Bedford, MA, USA).

2.2. Ultraperformance Liquid Chromatography (UPLC). UPLC was performed using the Waters ACQUITY system with photodiode array (PDA) detector and LCT premier™ Xe Mass Spectrometer (Waters Corporation, Milford, MA, USA). Clear solutions of 40 μg/ml of $G_{0\text{-}6}$ (C_2 and C_4) dendrimers were prepared in 90% of (0.1% trifluoroacetic acid (TFA) in DI water) and 10% of (0.08% TFA in acetonitrile (ACN)) solution. A 5 μl of each solution was injected using the gradient program in Table 1. The column used was ACQUITY UPLC ™ BEH C_{18}, 1.7 μm, 2.1 × 50 mm. Chromatograms were detected at λ =210 nm. To obtain the mass spectra, a capillary voltage of 2800-3300 W and a cone voltage of 150 V were used. For data acquisition, 0.01-second inter-scan delays, 400 to 3500 m/z, positive ion, and W-geometry mode were applied. The system was calibrated over 650–3500 m/z using a 0.4 mg/ml NaI solution. The calibration was confirmed to a 0.5-Da tolerance using an infusion of 80 μg/ml horse heart myoglobin (Mass 16,951.48 Da). A programmable syringe pump (Cole Parmer, Vernon Hills, IL) was used to apply an infusion rate of 120-500 μl/hr. Samples were identified based on their elution times (ET) and selected segments of their MS spectra were deconvoluted using the MaxEnt1 deconvolution algorithm (up to 23 iterations) by using a uniform Gaussian damage model with a half-height peak width of 0.17-0.26 Da.

Table 1: UPLC gradient program.

Time (min)	Flow rate (ml/min)	% (0.1% TFA in H_2O)	% (0.08% TFA in ACN)
Initial	0.2	90	10
1	0.1	90	10
5	0.1	80	20
9	0.1	25	75
10	0.3	90	10

3. Results

3.1. UPLC. The ion-pair reversed phase UPLC was applied to separate the hydrophilic G_0-G_6 (C_2 and C_4) PAMAM dendrimers on a hydrophobic (C_{18}) column. Elution was optimized by making hydrophobic dendritic complexes with TFA [20]. Figure 1 shows the PDA signals for (G_0-G_6) C_2 (left) and (G_0-G_6) C_4 (right) PAMAM dendrimers. Since the shapes of the UPLC peaks are dependent on the gradient elution program, the results presented in Figure 1 relate only to the operating conditions used in this study.

Generally, the elution times (ETs) of both C_2 and C_4 dendrimers increase, with their generation numbers increasing as shown in Table 2 and Figure 2. The presence of well-defined peaks confirms the relative purity of these molecules. However, the broadness of some main peaks (due to shoulders or tails) and the appearance of smaller peaks, either before or after the ETs of the principal molecules, suggest the presence of multiple components and/or defects (formation of loops, missing arms (R), and trailing generations) during the synthesis of full generation dendrimers. Some smaller peaks (due to defects) may be embedded within the peak of the main molecule when changes in their surface

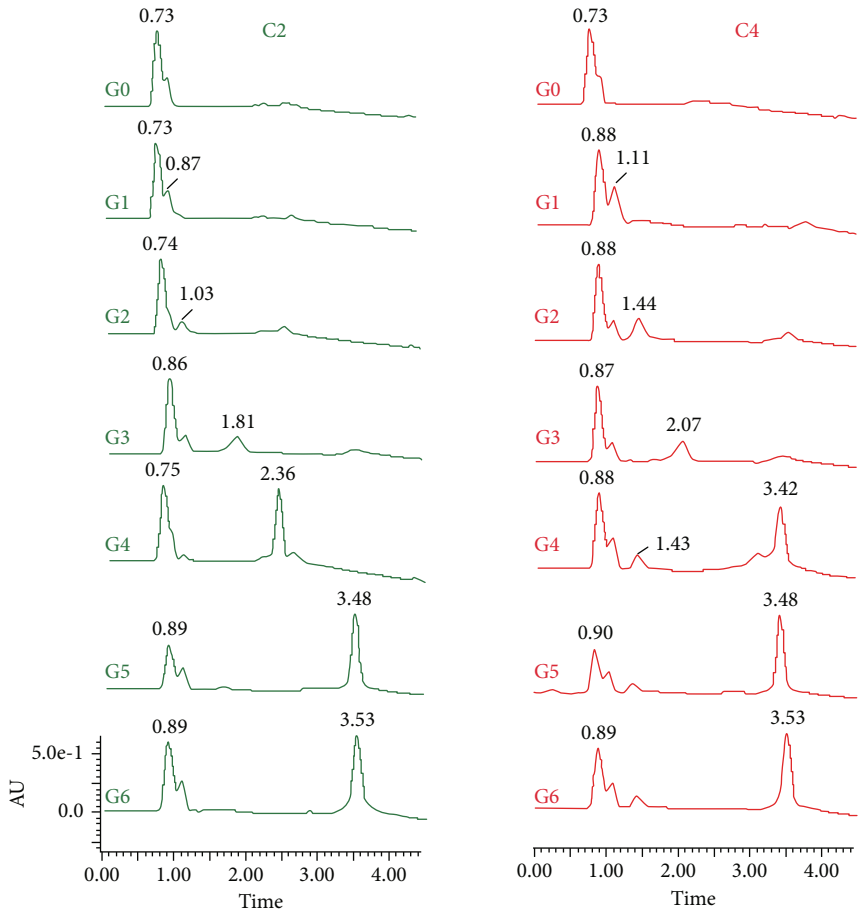

Figure 1: PDA signals for G_0-G_6 (C_2 and C_4) PAMAM dendrimers.

properties are not sufficient to cause significant differences in their ETs. These multiple peaks are indicators for molecular polydispersity's.

Figure 3 shows the first derivatives ($\Delta ET/\Delta G$) of the ETs for $G_{0\text{-}6}$ (C_2 and C_4) dendrimers. Generally, $\Delta ET/\Delta G$ gradually increases for C_2 dendrimers by increasing the generation number from G_0 to G_3 (with a sharp increase between G_2 and G_3). Then, a slight decrease in $\Delta ET/\Delta G$ was observed between G_3 and G_4 followed by another increase between G_4 and G_5 (this increase is < that between G_2 and G_3) and finally a very sharp decrease was seen between G_5 and G_6.

In contrast, different scenarios were seen for the more flexible C_4 dendrimers. For example, $\Delta ET/\Delta G$ gradually increases by increasing the generation number from G_0 to G_3 (with a slight increase between G_2 and G_3). Then, a sudden increase in $\Delta ET/\Delta G$ was seen between G_3 and G_4 followed by a very sharp decrease between G_4 and G_5 and finally a slight decrease between G_5 and G_6.

3.2. ESI-TOF-MS. The ESI-TOF-MS spectra were analyzed primarily to determine the structure of the main molecule and defects during synthesis. A detailed description of various structural defects and accompanying reaction schemes can be found in the work of Peterson et al. [21]. Strong, stable signals were readily obtained for all dendrimers (ranged in size from G_0C_2 (theoretical Mw = 517 Da) to G_6C_4 (theoretical Mw = 58,076 Da)). Table 3 shows the structure of the main molecules and defects during synthesis for G_0-G_3 (C_2 and C_4) dendrimers while Figure 4 depicts the ESI-TOF-MS spectra for their UPLC peaks. Figure 4(a), the m/z ion observed at 517.20, corresponds to the protonated molecule of the ideal (defect-free) structure (M) of G_0C_2 dendrimers with four amine terminal groups. The peak at m/z 539.21 is due to $[M+Na]^+$. Similarly, Figure 4(b) shows m/z ions

Table 2: ET and ($\Delta ET/\Delta G$) for G_0-G_6 (C_2 and C_4) PAMAM dendrimers.

Generation number	ET (min)		$\Delta ET/\Delta G$	
	C_2	C_4	C_2	C_4
0	0.88	0.87		
1	0.9	1.11	0.02	0.24
2	1.03	1.45	0.13	0.34
3	1.81	2.07	0.78	0.62
4	2.36	3.41	0.55	1.34
5	3.48	3.48	1.12	0.07
6	3.53	3.53	0.05	0.05

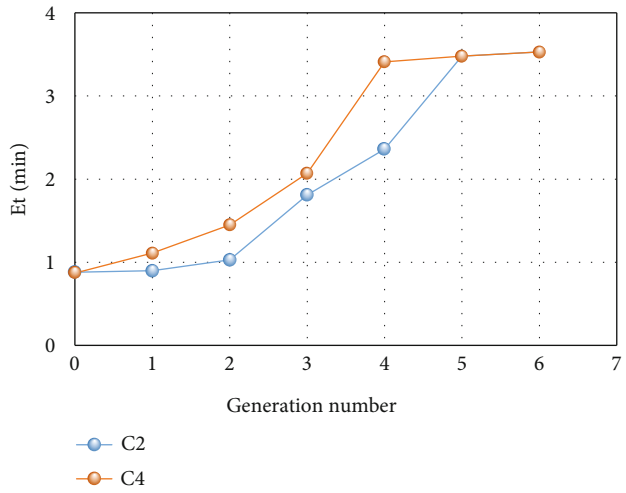

Figure 2: Elution times (ETs) for G_0-G_6 (C_2 and C_4) PAMAM dendrimers.

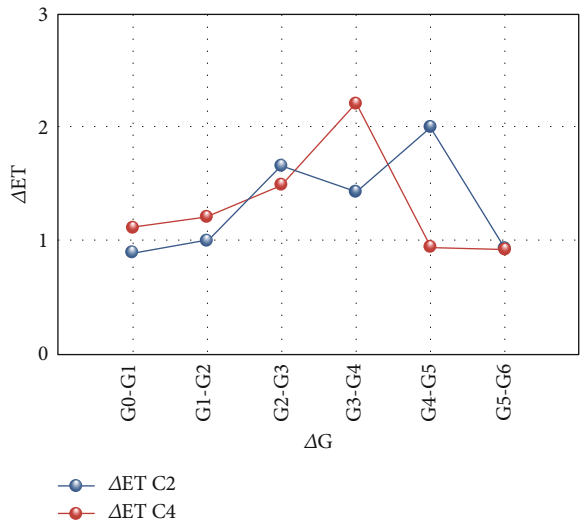

Figure 3: Intergenerational elution time differences (ΔET/ΔG) for G_0-G_6 (C_2 and C_4) PAMAM dendrimers.

at 545.22 and 567.23 that correspond to ideal (defect-free) structure of G_0C_4 and its Na salt, respectively.

Figure 4(c) depicts the ESI-TOF-MS peaks for G_1C_2 dendrimers where the $[M+H]^+$ ion of the molecule was shown at m/z 1429.58. Some of the peaks of lower molar masses of the ideal G_1C_2 molecule were formed due to incomplete Michael addition, resulting in asymmetric dendrimer structures. In general, the compound at m/z 1201.51 is showing two missing arms (-2R = -2 (R-$CH_2CH_2CONHCH_2CH_2NH_2$-, 114 Da)). Additionally, some ions with structural errors due to intramolecular cyclization or intermolecular dimer formation were obtained during the amidation step of G_1C_2 synthesis. For example, the peaks at m/z 1027.33 and 913.36 indicate the presence of molecules that have one loop (L, 60 Da) with three and four missing arms, respectively. Finally, the spectrum also shows a component at m/z

Table 3: The structure of the main molecules and defects during synthesis for G_0-G_3 (C_2 and C_4) dendrimers.

Generation	Molecule	Observed mass (Da)
0	$[G_0C_2+H]^{+1}$	517.20
	$[G_0C_2+Na]^{+1}$	539.27
	$[G_0C_4+H]^{+1}$	545.22
	$[G_0C_4+Na]^{+1}$	567.23
1	$[G_1C_2+H]^{+1}$	1429.58
	$[G_1C_2$-2R+H$]^{+1}$	1201.51
	$[G_1C_2$+1L-3R+H$]^{+1}$	1027.33
	$[G_1C_2$+1L-4R+H$]^{+1}$	913.36
	$[G_1C_2+2H]^{2+}$	715.28
	$[G_1C_4+H]^{+1}$	1457.63
	$[G_1C_4$-2R+H$]^{+1}$	1229.54
	$[G_1C_4$+1L-4R+H$]^{+1}$	941.39
	$[G_1C_{4+}$1L-4R+Na$]^{+1}$	963.37
	$[G_1C_4+2H]^{2+}$	729.32
2	$[G_2C_2+3H]^{3+}$	1085.00
	$[G_2C_2+2H+1TFA]^{2+}$	1685.00
	$[G_2C_2+2H+2TFA]^{2+}$	1742.00
	$[G_2C_2+2H+3TFA]^{2+}$	1799.00
	$[G_2C_4+2H]^{2+}$	1642.18
	$[G_2C_4+2H+1TFA]^{2+}$	1699.14
	$[G_2C_4+2H+1L+1TFA]^{2+}$	1384.05
	$[G_2C_4+3H]^{3+}$	1095.11
	$[G_2C_4+3H+2TFA]^{3+}$	1171.11
3	$[G_3C_2+6H]^{6+}$	1151.93
	$[G_3C_2+7H+1L-4R]^{7+}$	913.34
	$[G_3C_4+4H]^{4+}$	1734.22
	$[G_3C_4+5H]^{5+}$	1387.76
	$[G_3C_4+6H]^{6+}$	1156.64

715.28 which has exactly half the mass of the full generation of G_1C_2. This refers to the double charged $[M+2H]^{2+}$ions.

Figure 4(d) represents MS signals of G_1C_4. The signals were dominated by $[M+H]^{1+}$ ion observed at m/z 1457.63, while ions at m/z 1229.54, 941.39, 963.37, and 729.32 represent $[M-2R+H]^{1+}$, $[M+L-4R+H]^{1+}$, $[M+L-4R+Na]^{1+}$, and $[M+2H]^{2+}$, respectively.

Figure 4(e) depicts the G_2C_2 spectrum. The main structure ion is seen at m/z 1085 and represents $[M+3H]^{3+}$. TFA adducts were seen at m/z 1685, 1742, and 1799. They represent $[M+2H+$ (1, 2, and 3 TFA adducts)$]^{2+}$, respectively. Finally, the TFA adducts seen at m/z 1123 and 1237 represent $[M+3H+$ (1 and 4 TFA)$]^{3+}$, respectively.

Figure 4(f) shows the deconvoluted mass spectrum of the G_2C_2 where the molar mass of the main molecule appears at 3256.3 Da.

The mass spectrum for G_2C_4 is seen in Figure 4(g), and the spectrum represents $[M+2H]^{2+}$ at m/z 1642.18, $[M+2H+1TFA]^{2+}$at m/z 1699.14, $[M+2H+1L+1TFA]^{2+}$ at m/z 1384.05, $[M+3H]^{3+}$ at m/z 1095.11, and $[M+3H+2TFA]^{3+}$

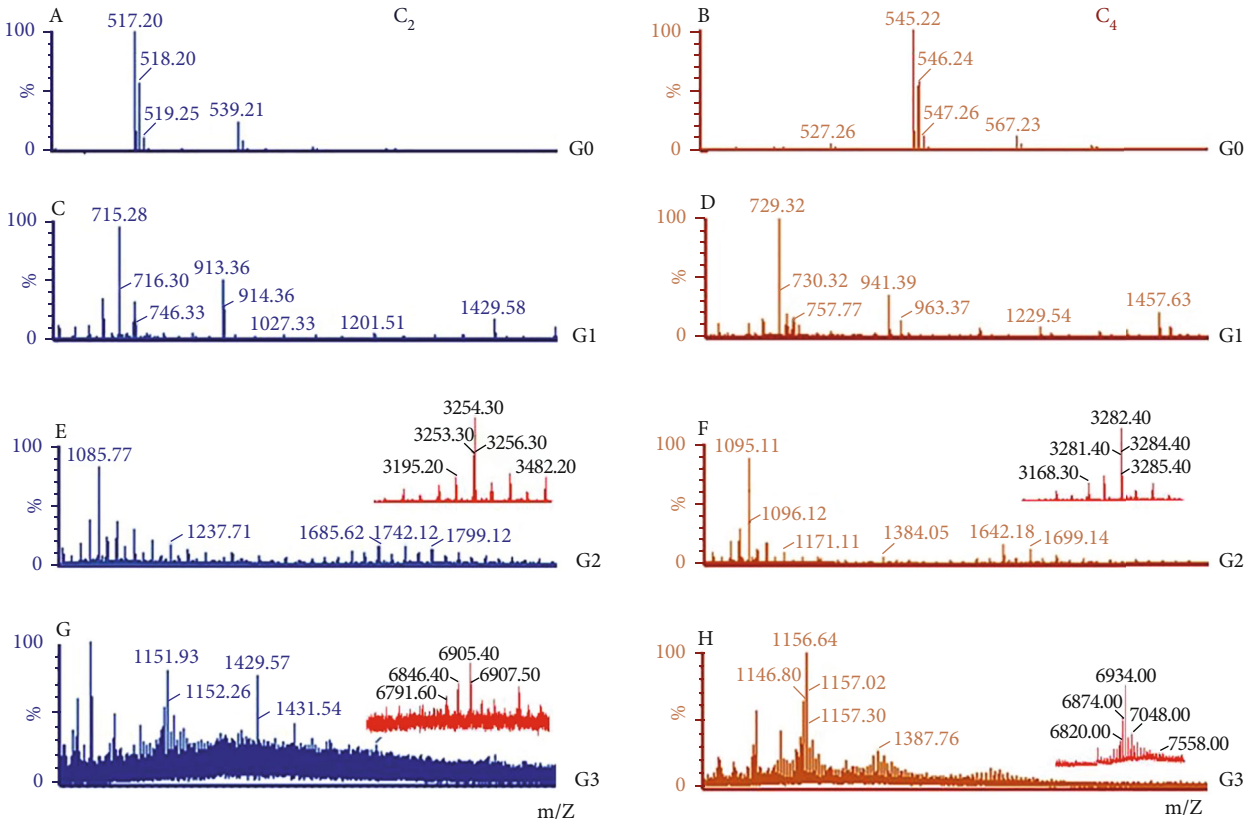

FIGURE 4: ESI-MS for UPLC peaks of G_0-G_3 (C_2 and C_4) PAMAM dendrimers.

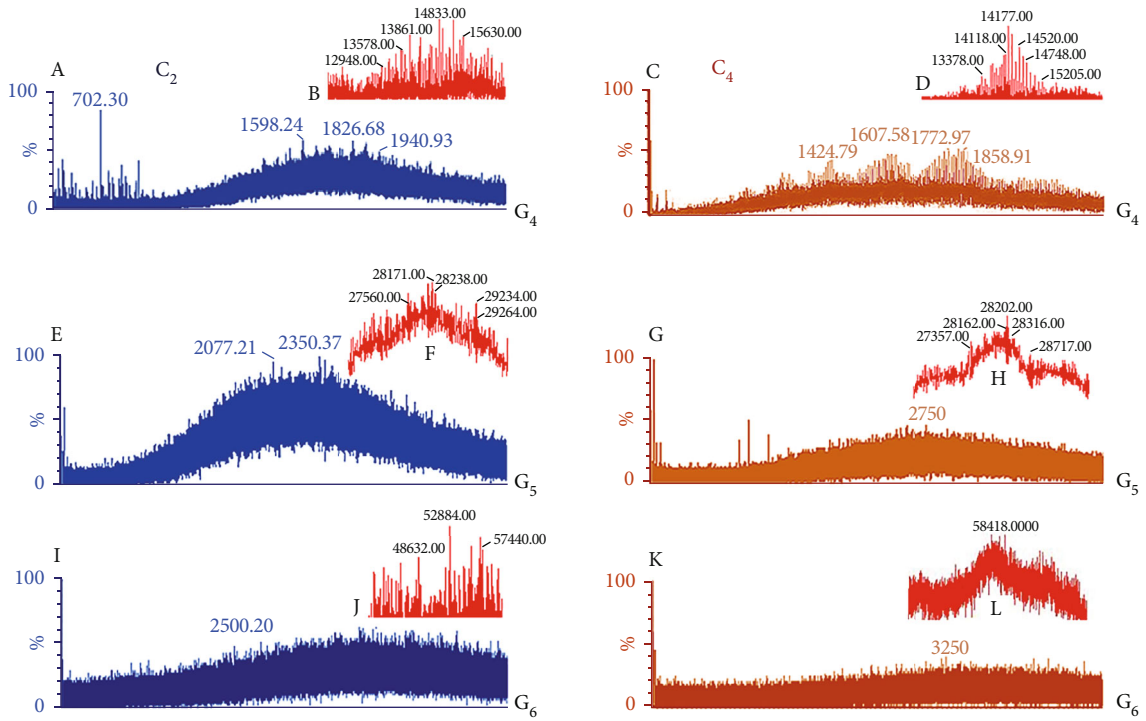

FIGURE 5: ESI-MS for UPLC peaks of G_4-G_6 (C_2 and C_4) PAMAM dendrimers.

at m/z 1171.11. The deconvoluted mass spectrum of G_2C_4 was shown in Figure 4(h) and the molar mass of the molecule was seen at 3284.4 Da.

Figure 4(i) represents MS signals for G_3C_2. Signals from the main molecule are seen at m/z 1151.93 and represent $[M+6H]^{6+}$. Accumulation of synthetic errors due to missing repeating units can lead to the formation of trimmed dendrimers with different amounts of low molecular weight fragments that causes the heterogeneity in the sample. This effect was demonstrated here at m/z 913.34 and was represented by $[M+7H+1L-4R]^{7+}$. Figure 4(j) shows the deconvoluted mass spectrum of the G_3C_2 at 6905.40 Da.

The spectrum of G_3C_4 is shown in Figure 4(k) where $[M+4H]^{4+}$, $[M+5H]^{5+}$, and $[M+6H]^{6+}$ were seen at m/z 1734.22, 1387.76, and 1156.64, respectively. The deconvoluted mass spectrum of G_3C_4, Figure 4(l), shows the main molecule at 6935.70 Da. The appearance of well-identified multiply charged ions confirms that G_3C_4 is cleaner than G_3C_2 dendrimers.

The peaks show the resolved intact molecules for $G_{0\text{-}3}$ (C_2 and C_4) PAMAM dendrimers at different charge states. The spectra also contain signals arising from the loss of at least one arm ((R) -CH2CH2CONHCH2CH2NH2, -114 Da) and formation of intramolecular loops (L, -60 Da).

The MS peaks of G_4C_2 dendrimers (theoretical Mw = 14215 Da) are shown in Figure 5(a). Important ions (11^+ to 6^+) consistent with the main molecule were observed. The deconvoluted mass spectrum of the G_4C_2 is shown in Figure 5(b). The charge-state distribution corresponding to this generation is hardly resolvable and is centered around 1800 m/z. Figure 5(c) shows the mass spectrum of G_4C_4 dendrimers (theoretical Mw = 14243 Da). Contrary to G_4C_2 dendrimers, the charge-state distribution corresponding to this generation (11^+ to 6^+) was highly resolvable and centered around 1800 m/z. This result indicates that more impurities, trapped within the dendritic particles, were successfully removed by the UPLC column prior to their detection by ESI-TOF-MS. Figure 5(d) shows that the deconvoluted results of G_4C_4 were cleaner than those of G_4C_2 dendrimers.

Figure 5(e) depicts the mass spectrum for the G_5C_2 dendrimers, theoretical Mw 28826 Da. The charge-state distribution (12^+) was seen centered around 2400 m/z. The deconvoluted results showed that the molecular weight of the G_5C_2 dendrimers is seen around 28000 Da, Figure 5(f). In contrast, the charge-state distribution corresponding to G_5C_4 dendrimers (13^+) was more resolvable than that for G_5C_2 dendrimers and was centered around 2400 m/z, Figure 5(g). The deconvoluted mass spectrum of the G_5C_4 dendrimers was depicted in Figure 5(h) and the mass of the molecule was seen around 28200 Da.

As the generation of the dendrimers increases to G_6 (theoretical Mw, =58048 Da for C_2 and 58076 Da for C_4), the sample detection appears at higher m/z, with the center of the peak for the G_6C_2 dendrimer being detected at 3400 m/z, Figure 5(i), and charge-state distribution of (17^+). In contrast, the charge-state distribution corresponding to G_6C_4 dendrimers (18^+) was more resolvable than that of G_6C_2 dendrimers and centered around m/z 3226 (Figure 5(j)).

4. Discussions

Figure 1 shows the PDA signals for (G_0-G_6) C_2 (left) and (G_0-G_6) C_4 (right) PAMAM dendrimers. Generally, ETs for both dendritic cores increase with the increase in their generation numbers as shown in Table 2 and in Figure 2. Since the theoretical charge-to-mass ratio from generation to generation remains constant for both dendritic cores, then the main factor governing their chromatographic elution is the surface ion-pair density [20]. This ion-pair density increases with the increase in generation number leading to an increase in the molecular hydrophobicity and hence an increase in the molecular ETs [20]. Another parameter that may affect the ETs, based on our study, is the core length. For example, the core length of C_4 dendrimers is almost twice the core length of C_2 dendrimers. The increase in the core length of C_4 increases the hydrophobicity of the C_4 core itself and increases the relative flexibility of the entire molecule as well. This relative molecular flexibility in turn has most likely allowed the early generations of C_4 dendrimers "more flexible" to expose the majority of their hydrophobic interiors to the hydrophobic C_{18} column leading to an increase in their ETs when compared to the ETs of the same generations of C_2 dendrimers. This behavior was confirmed in this study for generations $G_{1\text{-}3}$ (C_4).

Theoretically, the ratio of the molecular weight (Mw) of the core to the total Mw of the entire dendritic molecule, for both C_2 and C_4 dendrimers, decreases by increasing their generation numbers. Similarly, the ratio of the core length to the diameter of the entire dendritic molecules decreases by increasing their generation numbers. This fact leads to the expectation that the largest difference in the ETs between C_2 and C_4 dendrimers can be seen between G_0C_2 and G_0C_4 dendrimers. Contrary to this expectation, we found that the ETs of both G_0C_2 (0.88 min) and G_0C_4 (0.87 min) dendrimers were nearly similar and that both were eluted very early from the column. This result could be attributed to the fact that both cores have very small elution volumes and that these elution volumes are insufficient to distinguish between these two small dendrimer molecules according to our elution program.

Figure 3 shows the first derivatives of the ETs ($\Delta ET/\Delta G$) for $G_{0\text{-}6}$ (C_2 and C_4) dendrimers. Generally, the $\Delta ET/\Delta G$ of C_2 dendrimers increases by increasing their generation number from G_0 to G_3. These early generations of dendrimers show very open molecular structures [22]. Thus, both the mobile phase and the hydrophobic column can access the dendritic cores and their inner branches. Accordingly, the ETs of these dendrimers depend on both the lengths of their dendritic cores and on their entire dendritic volumes. However, a significant early increase in the $\Delta ET/\Delta G$ was observed between G_2 and G_3 dendrimers. This can be attributed to the early transition from an accessible open core region to a relatively confined region while the dendrimer benches are still accessible. Next, a decrease in the $\Delta ET/\Delta G$ is observed between G_3 and G_4. It seems most likely that the dendritic branches have started to pack. A further increase in the $\Delta ET/\Delta G$ was then observed between G_4 and G_5 dendrimers followed by a very sharp decrease in

the $\Delta ET/\Delta G$ between G_5 and G_6 dendrimers. These indicate that the dendritic molecules became more compartmentalized, with the core region gradually being shielded off from the surrounding mobile phase by the outer shell growing to become much more molecularly dense [13]. In this case, the gradually growing molecular surface area, rather than the molecular volume or core length, mainly controls the ET. This expectation is supported by the results of Goddard, Turro, Watkins, Tomalia, and their groups who find that the effective extent of hydrophobicity provided by the core depends not only on the length of the core but on the magnitude of generation size as well [11, 13, 22, 23].

In contrast, different scenarios were seen for the more flexible C_4 dendrimers. For example, the $\Delta ET/\Delta G$ gradually increases by increasing the generation number from G_0 to G_3. Then, a sudden increase in the $\Delta ET/\Delta G$ was seen for dendrimer moving from G_3 to G_4 followed by a sharp decrease in $\Delta ET/\Delta G$ between G_4 and G_5 dendrimers and finally a slight decrease in $\Delta ET/\Delta G$ between G_5 and G_6 dendrimers. This result could be inferred as follows: the core length of the highly open molecular structures of $G_{0\text{-}3}$ dendrimers mostly drove the ET. In contrast, both the length of the C_4 core and the intermediate rigidity/elasticity of its entire molecule control the ET. Beyond G_4, the molecular packing prompted a change in the dendrimer profile with the development of nanocontainer properties. Therefore, ET mostly became dominated by the stiffness of the whole molecule following the same scenario for C_2 dendrimers. Finally, although, G_6C_4 is relatively more rigid than G_5C_4 dendrimers; however, no significant differences were found in their ETs likely due to our column/elution program setup.

Overall, C_4 dendrimers were generally found to be cleaner than C_2 dendrimers. This can be understood as follows: application of TFA resulted in an acidic mobile phase of pH <2.5 leading to the protonation of both primary (pKa =9-10) and tertiary amines (pKa =4-5) [24]. Protonation of these amines leads to a 4D molecular swelling (4D = changes in the 3D molecular profiles of dendrimers over time due to change in the elution program and hence change in pH) of dendritic molecules within the column, throughout the entire elution period, of both C_4 and C_2 dendrimers. The 4D swelling of C_4 dendrimers (larger core length) is expected to be greater than that of C_2 dendrimers. This larger swilling facilitates the removal of the trapped impurities from the C_4 dendrimer molecules. These impurities were then easily separated by the UPLC column leading to missy UPLC chromatograms while producing clear MS spectra. In contrast, the length of the C_2 core is approximately half the length of the C_4 core dendrimers. Accordingly, C_2 has generally produced stiffer dendrimers. This effect is expected to moderate the role of the solvent and reduce the 4D swilling of the dendrimer [22]. Thus, large amounts of impurities remain trapped within the C_2 dendrimers. These impurities cannot be easily differentiated by the UPLC column (according to our setup). Thus, clean chromatograms are produced where the impurity curves hide within the curves of the molecules. When these molecules reach the MS, they are detected and shown as missy spectra.

5. Conclusions

We presented a fast sensitive UPLC-ESI-TOF-MS method to separate, detect, and differentiate between seven $G_{0–6}$ generations of C_4 and C_2 dendrimers. Charge-state distributions as high as (18^+) and m/z 3226 are revealed for dendrimers that have a theoretical Mw of ca half mega Dalton. C_4 dendrimers are found to be more pure than C_2 dendrimers. This result is attributed to the flexibility of the C_4 dendrimers (due to their longer core length) compared to C_2 dendrimers. This relative flexibility enabled the C_4 dendrimers to have more molecular swilling, due to the pH of the mobile phase, than the C_2 dendrimers and as a result release more trapped impurity. The change in profile occurs from expanded compressible molecules in the early generations $G_{(0\ -3)}$ to more rigid globular shapes in the later generations $G_{(5,\ 6)}$. In contrast, critical generations, G =3–4, behave more like an Einstein spheroid [25]. Finally, it is worthy to mention that some impurities may not leave the system under our experimental conditions. Thus, dialysis is recommended to remove significant traces of starting materials from dendrimers prior to their use. This will provide cleaner dendrimers and reduce toxicity due to starting materials [26].

Data Availability

The data used to support the findings of this study are available from the corresponding author upon request.

Conflicts of Interest

The authors declare that they have no known competing financial interests or personal relationships that could have appeared to influence the work reported in this paper.

Authors' Contributions

Hosam Gharib Abdelhady is responsible for conceptualization, data curation, investigation, validation, formal analysis, funding acquisition, writing – original draft. Fadilah Sfouq Aleanizy is responsible for investigation, validation, writing – original draft, formal analysis. Fulwah Yahya Alqahtanic is responsible for writing – review and editing. Hamad M. Alkahtanid is responsible for the software.

Acknowledgments

This research was partially funded by the King Abdulaziz City for Science and Technology and its National Science, Technology, and Innovation Plan under Award # 13-NAN34-05 (Via Science and Technology Unit, Taibah University, Al-Madinah Al-Munawwarah, KSA).

Supplementary Materials

Graphical Abstract: a) UPLC columns eluting G_3C_4 (left) and G_3C_2 (right) PAMAM dendrimers. The influx of impurities from the inner nanocavities of G_3C_4 is more than the influx of impurities from the inner nanocavities of G_3C_2 dendrimers. b) Red is the chromatogram of G_3C_4 and green

is the chromatogram of G_3C_2. No significant differences are seen in their chromatograms. c) Brown is the mass spectrum of G_3C_4, and blue is the mass spectrum of G_3C_2. The appearance of well-identified multiply charged ions in the brown spectrum confirms that G_3C_4 is cleaner than G_3C_2 dendrimers. *(Supplementary Materials)*

References

[1] D. A. Tomalia, H. Baker, J. Dewald et al., "A new class of polymers: starburst-dendritic macromolecules," *Polymer Journal*, vol. 17, no. 1, pp. 117–132, 1985.

[2] B. Srinageshwar, S. Peruzzaro, M. Andrews et al., "PAMAM dendrimers cross the blood–brain barrier when administered through the carotid artery in C57BL/6J mice," *International Journal of Molecular Sciences*, vol. 18, no. 3, p. 628, 2017.

[3] H. G. Addelhady, "Direct real-time molecular scale visualisation of the degradation of condensed DNA complexes exposed to DNase I," *Nucleic Acids Research*, vol. 31, no. 14, pp. 4001–4005, 2003.

[4] A. U. Bielinska, C. Chen, J. Johnson, and J. R. Baker, "DNA complexing with polyamidoamine dendrimers: implications for transfection," *Bioconjugate Chemistry*, vol. 10, no. 5, pp. 843–850, 1999.

[5] J. Haensler and F. C. Szoka, "Polyamidoamine cascade polymers mediate efficient transfection of cells in culture," *Bioconjugate Chemistry*, vol. 4, no. 5, pp. 372–379, 1993.

[6] J. F. Kukowska-Latallo, A. U. Bielinska, J. Johnson, R. Spindler, D. A. Tomalia, and J. R. Baker Jr., "Efficient transfer of genetic material into mammalian cells using Starburst polyamidoamine dendrimers," *Proceedings of the National Academy of Sciences of the United States of America*, vol. 93, no. 10, pp. 4897–4902, 1996.

[7] A. M. Caminade, C. O. Turrin, and J. P. Majoral, "Dendrimers and DNA: combinations of two special topologies for nanomaterials and biology," *Chemistry - A European Journal*, vol. 14, no. 25, pp. 7422–7432, 2008.

[8] L. D. Margerum, B. K. Campion, M. Koo et al., "Gadoliniu-m(III) DO3A macrocycles and polyethylene glycol coupled to dendrimers effect of molecular weight on physical and biological properties of macromolecular magnetic resonance imaging contrast agents," *Journal of Alloys and Compounds*, vol. 249, no. 1-2, pp. 185–190, 1997.

[9] M. R. Knecht and D. W. Wright, "Amine-terminated dendrimers as biomimetic templates for silica nanosphere formation," *Langmuir*, vol. 20, no. 11, pp. 4728–4732, 2004.

[10] D. A. Tomalia, "Dendrons/dendrimers: quantized, nanoelement like building blocks for soft-soft and soft-hard nanocompound synthesis," *Soft Matter*, vol. 6, no. 3, pp. 456–474, 2010.

[11] A. M. Naylor, W. A. Goddard, G. E. Kiefer, D. A. Tomalia, and S. Dendrimers, "Starburst dendrimers. 5. Molecular shape control," *Journal of the American Chemical Society*, vol. 111, no. 6, pp. 2339–2341, 1989.

[12] D. A. Tomalia, "Starburst/cascade dendrimers: fundamental building blocks for a new nanoscopic chemistry set," *Advanced Materials*, vol. 6, no. 7-8, pp. 529–539, 1994.

[13] D. A. Tomalia, A. M. Naylor, and W. A. Goddard, "Starburst dendrimers: molecular-level control of size, shape, surface chemistry, topology, and flexibility from atoms to macroscopic matter," *Angewandte Chemie International Edition in English*, vol. 29, no. 2, pp. 138–175, 1990.

[14] C. A. Cason, S. A. Oehrle, T. A. Fabré et al., "Improved methodology for monitoring poly(amidoamine) dendrimers surface transformations and product quality by ultra performance liquid chromatography," *Journal of Nanomaterials*, vol. 2008, Article ID 456082, 7 pages, 2008.

[15] H. Gharib Abdelhady, "Fast sensitive UPLC electro spray ionization time of flight mass spectroscopy determination of diethanolamine in small dendritic nanomolecules," *Journal of Taibah University Medical Sciences*, vol. 6, no. 2, pp. 86–92, 2011.

[16] M. A. van Dongen, S. Vaidyanathan, and M. M. Banaszak Holl, "PAMAM dendrimers as quantized building blocks for novel nanostructures," *Soft Matter*, vol. 9, no. 47, p. 11188, 2013.

[17] M. I. Churchwell, N. C. Twaddle, L. R. Meeker, and D. R. Doerge, "Improving LC-MS sensitivity through increases in chromatographic performance: comparisons of UPLC-ES/MS/MS to HPLC-ES/MS/MS," *Journal of Chromatography BLife Sciences*, vol. 825, pp. 134–143, 2005.

[18] B. Baytekin, N. Werner, F. Luppertz et al., "How useful is mass spectrometry for the characterization of dendrimers?: "Fake defects" in the ESI and MALDI mass spectra of dendritic compounds," *International Journal of Mass Spectrometry*, vol. 249-250, pp. 138–148, 2006.

[19] B. L. Schwartz, A. L. Rockwood, R. D. Smith, D. A. Tomalia, and R. Spindler, "Detection of high molecular weight starburst dendrimers by electrospray ionization mass spectometry," *Rapid Communications in Mass Spectrometry*, vol. 9, no. 15, pp. 1552–1555, 1995.

[20] M. T. Islam, X. Shi, L. Balogh, and J. R. Baker, "HPLC separation of different generations of poly(amidoamine) dendrimers modified with various terminal groups," *Analytical Chemistry*, vol. 77, no. 7, pp. 2063–2070, 2005.

[21] J. Peterson, V. Allikmaa, J. Subbi, T. Pehk, and M. Lopp, "Structural deviations in poly(amidoamine) dendrimers: a MALDI-TOF MS analysis," *European Polymer Journal*, vol. 39, no. 1, pp. 33–42, 2003.

[22] P. K. Maiti, T. Çağin, G. Wang, and W. A. Goddard, "Structure of PAMAM dendrimers: generations 1 through 11," *Macromolecules*, vol. 37, no. 16, pp. 6236–6254, 2004.

[23] D. M. Watkins, Y. Sayed-sweet, J. W. Klimash, N. J. Turro, and D. A. Tomalia, "Dendrimers with hydrophobic cores and the formation of supramolecular dendrimer-surfactant assemblies," *Langmuir*, vol. 13, no. 12, pp. 3136–3141, 1997.

[24] Y. Mengerink, M. Mure, E. M. M. De Brabander, and S. Van Der Wal, "Exclusion chromatography of polypropylenamine dendrimers," *Journal of Chromatography A*, vol. 730, no. 1-2, pp. 75–81, 1996.

[25] D. A. Tomalia, J. B. Christensen, and U. Boas, "Dendrimers, Dendrons, and Dendritic Polymers, Discovery, Applications, and the Future," Cambridge Univ. Press, 2012.

[26] H. G. Abdelhady, H. A. Abdel-Salam, E. M. Niazy et al., "Spatiotemporal PFQNM visualization of the effect of suicide dendriplexes on dividing HeLa cells," *Biologie et Médecine*, vol. 12, no. 8, pp. 2365–2371, 2016.